Spin Asymmetries of the Nucleon Experiment

W. Armstrong,[1,2] H. Kang,[3] A. Liyanage,[4] J. Maxwell,[5] J. Mulholland,[6] L. Ndukum,[7] A. Ahmidouch,[8] I. Albayrak,[4] A. Asaturyan,[9] O. Ates,[4] H. Baghdasaryan,[6] W. Boeglin,[10] P. Bosted,[5] E. Brash,[11,12] C. Butuceanu,[13] M. Bychkov,[6] P. Carter,[11] C. Chen,[4] J.-P. Chen,[5] S. Choi,[3] M.E. Christy,[4] S. Covrig,[5] D. Crabb,[6] S. Danagoulian,[8] A. Daniel,[14] A.M. Davidenko,[15] B. Davis,[8] D. Day,[6] W. Deconink,[5] A. Deur,[5] J. Dunne,[7] D. Dutta,[7] L. El Fassi,[16] C. Ellis,[5] R. Ent,[5] D. Flay,[1] E. Frlez,[6] D. Gaskell,[5] O. Geagla,[6] J. German,[8] R. Gilman,[16] J. Gomez,[5] Y.M. Goncharenko,[15] O. Hashimoto,[17] D. Higinbotham,[5] T. Horn,[5] G. Huber,[13] M. Jones,[8] M.K. Jones,[5] N. Kalantarians,[18] H-K. Kang,[3] D. Kawama,[17] C. Keith,[5] C. Keppel,[4] M. Khandaker,[19] Y. Kim,[3] P.M. King,[14] M. Kohl,[4] K. Kovacs,[6] V.I. Kravtsov,[15] V. Kubarovsky,[20] Y. Li,[4] N. Liyanage,[6] W. Luo,[21] D. Mack,[5] V. Mamyan,[6] P. Markowitz,[10] T. Maruta,[17] D. Meekins,[5] Y.M. Melnik,[15] Z.-E. Meziani,[1] A. Mkrtchyan,[9] H. Mkrtchyan,[9] V.V. Mochalov,[15] P. Monaghan,[4] A. Narayan,[7] S. Nue Nakamura,[17] A. Nuruzzaman,[7] L. Pentchev,[22] D. Pocanic,[6] M. Posik,[1] A. Puckett,[23] X. Qiu,[4] J. Reinhold,[10] S. Riordan,[6] J. Roche,[14] O.A. Rondón,[6] B. Sawatzky,[1] M. Shabestari,[6] K. Slifer,[24] G. Smith,[5] L. Soloviev,[15] P. Solvignon,[2] V. Tadevosyan,[9] L. Tang,[4] G. Toshiyuki,[17] A. Vasiliev,[15] M. Veilleux,[11] T. Walton,[4] F. Wesselmann,[25] S. Wood,[5] H. Yao,[1] Z. Ye,[4] and L. Zhu[4]

(SANE Collaboration)

[1]*Temple University, Philadelphia, PA*
[2]*Argonne National Laboratory, Argonne, IL*
[3]*Seoul National University, Seoul, Korea*
[4]*Hampton University, Hampton, VA*
[5]*Thomas Jefferson National Accelerator Facility, Newport News, VA*
[6]*University of Virginia, Charlottesville, VA*
[7]*Mississippi State University, Jackson, MI*
[8]*North Carolina A&M State University, Greensboro, NC*
[9]*Yerevan Physics Institute, Yerevan, Armenia*
[10]*Florida International University, Miami, FL*
[11]*Christopher Newport University, Newport News, VA*
[12]*Thomas Jefferson National Accelerator Facility, Newport News, VA*
[13]*University of Regina, Regina, SK*
[14]*Ohio University, Athens, OH*
[15]*Institute for High Energy Physics, Protvino, Moscow Region, Russia*
[16]*Rutgers University, New Brunswick, NJ*
[17]*Tohoku U. Tohoku, Japan*
[18]*Virginia Union University, Richmond, VA*
[19]*Norfolk State University, Norfolk, VA*
[20]*Rensselaer Polytechnic Institute, Troy, NY*
[21]*Lanzhou University, Lanzhou 730000, Gansu, People's Republic of China*
[22]*College of William and Mary, Williamsburg, VA*
[23]*University of Connecticut, Storrs, CT*
[24]*University of New Hampshire, Durham, NH*
[25]*Xavier University, New Orleans, LA*

(Dated: April 24, 2018)

The Spin Asymmetries of the Nucleon experiment (SANE) measured two double spin asymmetries using a polarized proton target and polarized electron beam at two beam energies, 4.7 GeV and 5.9 GeV. A large-acceptance open-configuration detector package identified scattered electrons at 40° and covered a wide range in Bjorken x ($0.3 < x < 0.8$). Proportional to an average color Lorentz force, the twist-3 matrix element, $\tilde{d}_2^p$, was extracted from the measured asymmetries at Q^2 values ranging from 2.0 to 6.0 GeV^2. The results are found to be in agreement with the existing measurements and lattice QCD calculations, however, the observed salient scale dependence of $\tilde{d}_2$ deserves further investigation.

Today, it is accepted that Quantum Chromodynamics (QCD), the gauge theory of strong interactions, plays a central role in our understanding of nucleon structure at the heart of most visible matter in the universe. QCD successfully describes many observables in high energy scattering processes where the coupling among the confined constituents of hadrons (quarks and gluons) is small and perturbative (pQCD) calculations are possible, taking advantage of factorization theorems and evolution equations similar to quantum electrodynamics (QED). At the same time QCD offers a clear path to unravel the non-perturbative structure of hadrons using lattice QCD, a powerful *ab initio* numerical method that provides the best insight when the coupling among the constituents is strong.

The most fascinating property of QCD is confinement which must arise from the dynamics of the partons inside hadrons. A small window into this dynamical behavior is offered by observables sensitive to quark-gluon correlations inside the spin half nucleon. An operator product expansion (OPE) provides well-defined quantities which codify not only the well known parton distributions in the nucleon, but also quark-gluon correlations lacking a naive partonic interpretation. Taking advantage of the spin half of the nucleon, these quantities can be measured in polarized inclusive deep inelastic electron scattering experiments and calculated as well using lattice QCD (for review see[1]).

The principal focus of this Letter is the measurement of the dynamical twist-3 matrix element, $\tilde{d}_2$, which is interpreted as an average transverse color Lorentz force [2, 3] a quark feels as it starts its journey trying to escape the nucleon and becomes a hadron just as it is struck by the virtual photon during the scattering process. Most importantly, a transversely polarized nucleon target probed with polarized electrons yield a *unique* experimental situation where this color Lorentz force can be directly measured and used to test *ab initio* lattice QCD calculations.

The nucleon spin structure functions, g_1 and g_2, parameterizes the asymmetric part of the hadronic tensor, which through the optical theorem, is related to the forward virtual Compton scattering amplitude, $T_{\mu\nu}$. The reduced matrix elements of the quark operators appearing in the OPE analysis of $T_{\mu\nu}$ are related to Cornwall-Norton (CN) moments of the spin structure functions. At next-to-leading twist, the CN moments give

$$\int_0^1 x^{n-1} g_1(x,Q^2)dx = a_n + \mathcal{O}(\frac{M^2}{Q^2}), \quad n = 1,3,\ldots \tag{1}$$

and

$$\int_0^1 x^{n-1} g_2(x,Q^2)dx = \frac{n-1}{n}(d_n - a_n) + \mathcal{O}(\frac{M^2}{Q^2}), \quad n = 3,5,\ldots \tag{2}$$

where $a_n = \tilde{a}_{n-1}/2$ and $d_n = \tilde{d}_{n-1}/2$ are the twist-2 and twist-3 reduced matrix elements, respectively, which for increasing values of n have increasing dimension and spin.

If target mass corrections (TMCs) are neglected, the twist-3 matrix element can be extracted from the $n = 3$ CN moments at fixed Q^2

$$\tilde{d}_2 = \int_0^1 x^2\left(3g_T(x) - g_1(x)\right)dx \tag{3}$$

where $g_T = g_1 + g_2$. Using the so-called *Lorentz invariance relations* (LIR) and *equations of motion* (EOM) relations [4] the structure function can be written

$$g_T(x) = \frac{1}{2}\sum_a e_a^2 \Bigg[\Big\{\widetilde{g}^a_T(x) - \int_x^1 \frac{dy}{y}\Big(\widetilde{g}^a_T(y) + \widehat{g}^a_T(y)\Big)\Big\} + \Big\{\frac{m}{M}\frac{h_1^a(x)}{x} - \int_x^1 \frac{dy}{y}\Big(g_1^a(y) + \frac{m}{M}\frac{h_1^a(y)}{y}\Big)\Big\}\Bigg] \tag{4}$$

where the first braced term is pure twist-3 while the second is pure twist-2. The distributions $\widehat{g}_T$ and $\widetilde{g}_T$ are defined in the through the twist-3 quark-gluon-quark correlator. The former appears in the LIR while the latter comes from the EOM relations. The transversity distribution, h_1, disappears if the quark mass is neglected, i.e., $m \to 0$.

The $\tilde{d}_2$ matrix element is of particular interest because of its interpretation as a transverse average color Lorentz force acting on the struck quark the instant it is struck by the virtual photon [2, 3]. This can be easily seen by examining the Lorentz components of the gluon field strength tensor

$$G^{+y} = \frac{g}{\sqrt{2}}\left[\vec{E} + \vec{v}\times\vec{B}\right]^y = \frac{g}{\sqrt{2}}\left[E_y + B_x\right] \tag{5}$$

which appears in the definition of the local matrix element

$$\begin{aligned} F^y &= -\frac{\sqrt{2}}{2P^+}\langle P,S\left|\bar{q}(0)G^{+y}(0)\gamma^+ q(0)\right|P,S\rangle \\ &= -2M^2\tilde{d}_2\ . \end{aligned} \tag{6}$$

where this semi-classical interpretation is valid in the infinite momentum frame of the proton which is moving with velocity $\vec{v} = -c\hat{z}$.

Because both twist-2 and twist-3 operators contribute at the same order in transverse polarized scattering, a measurement of g_2 provides *direct* access to higher twist effects[5], i.e., without complicating fragmentation functions that are found in SIDIS experiments for example. This puts polarized DIS in an entirely unique situation to test lattice QCD [6] and models of higher twist effects.

The Spin Asymmetries of the Nucleon Experiment was conducted at Jefferson Lab in Hall-C during the winter of 2008-2009 using a longitudinally polarized electron beam and a polarized proton target. Inclusive inelastic electromagnetic scattering data in the regions of deep inelastic scattering and nucleon resonances were taken with two beam energies, $E = 4.7$ and 5.9 GeV, and with two target polarization directions: longitudinal, where the polarization direction was along the direction of the electron beam, and transverse, where the target polarization pointed in a direction perpendicular to the electron beam. To detect electrons at similar kinematics for both target configurations the magnet angle for the transverse configuration was 80°. Scattered electrons were detected in a new detector stack called the big electron telescope array (BETA) and also independently in Hall-C's high momentum spectrometer (HMS). Here we give a brief discussion of the experimental apparatus and techniques, which are discussed in more details in an instrumentation paper [7].

The beam polarization was measured periodically using a Møller polarimeter and production runs had beam polarizations from 60% up to 90%. The beam helicity was flipped from parallel to anti-parallel at 30 Hz and the helicity state, determined at the accelerator's injector, was recorded for each event.

A polarized ammonia target acted as an effective polarized proton target and achieved an average polarization of 68% by dynamic nuclear polarization in a 5 T field. NMR measurements, calibrated against the calculable thermal equilibrium polarization, provided a continuous monitor of the target polarization. To mitigate local heating and depolarizing effects, the beam current was limited to 100 nA and a raster system moved the beam in a 1 cm radius spiral pattern.By adjusting the microwave pumping frequency the proton polarization direction was reversed. These two directions, positive and negative target polarizations, were used to estimate associated systematic uncertainties, since taking equal amounts of data with alternating positive and negative target polarization largely cancels any correlated behavior in the sum.

BETA consisted of four detectors: a forward tracker placed close to the target, a threshold gas Cherenkov counter, a Lucite hodoscope, and a large electromagnetic calorimeter called BigCal. BETA was placed at a fixed central scattering angle of 40° and covered a solid angle of roughly 200 msr. Electrons were identified by the Cherenkov counter which had an average signal of roughly 18 photoelectrons[8]. The energy was determined by the BigCal calorimeter which consisted of 1744 lead glass blocks placed 3.35 m from the target. BigCal was calibrated using a set of $\pi^0 \to \gamma\gamma$ events. The Lucite hodoscope provided additional timing and position event selection cuts and the forward tracker was not used in the analysis of production runs.

The 5 T polarized-target magnetic field caused large deflections for charged particle tracks. In order to reconstruct tracks at the primary scattering vertex, corrections to the momentum vector reconstructed at BigCal were calculated from a set of neural networks that were trained with simulated data sets for each configuration.

The invariant mass of the unmeasured final state is $W = \sqrt{(}M^2 + 2M\nu - Q^2$ where M is the proton mass, $\nu = E - E'$ is the virtual photon energy, and $Q^2 = -q^2 = 2EE'(1 - \cos\theta)$. The scattered electron energy (E') and angle (θ) are used to calculate the Bjorken x variable $x = Q^2/2M\nu$. BETA's large solid angle and open configuration allowed a broad kinematic range ¿ in x and Q^2 to be covered in a single setting.

The measured double spin asymmetries for longitudinal ($\alpha = 180°$) and transverse ($\alpha = 80°$) target configurations were formed using the yields for beam helicities pointing along (+) and opposite (−) the direction of the electron beam,

$$A_m(\alpha) = \frac{1}{f(W,Q^2)P_B P_T}\left[\frac{N_+ - N_-}{N_+ + N_-}\right] \quad (7)$$

where $\alpha = 180°$ or $80°$ for the longitudinal and transverse target configurations respectively. The normalized yields are $N_\pm = n_\pm/(Q_\pm L_\pm)$ where $n_\pm$ is the raw number of counts for each run ($\sim$ 1 hour of beam on target), $Q_\pm$ is the accumulated charge for the given beam helicity over the counting period, and $L_\pm$ is the live time for each helicity, $f(W,Q^2)$ is the target dilution factor, and the beam and target polarizations are P_B and P_T respectively. The target dilution factor takes into account scattering from unpolarized nucleons in the target and depends on the scattered electron kinematics. It's discussed in detail in[7].

The dominant source of background for this experiment came from the decay of π^0s into two photons which, subsequently, produce electron-positron pairs which are then identified as DIS electrons. A pair produced outside of the target no longer experiences a strong magnetic field deflection, and therefore the pair travels in nearly the same direction. These events produced twice the amount of Čerenkov light and are effectively removed with an upper ADC cut[8]. However, pairs produced inside the target are sufficiently and oppositely deflected causing BETA to observe only one particle in the pair. These events cannot be removed through selection cuts and are treated through a background correction.

The background correction was determined by fitting existing inclusive π^0 production data and running a simulation to determine their contribution relative to the real inclusive electron scattering. The correction only becomes significant at scattered energies below 1.2 GeV where the positron-electron ratio begins to rise. The background correction consisted of a dilution (f_{BG}) and contamination (C_{BG}) term defined as

$$A_b(\alpha) = A_m(\alpha)/f_{\mathrm{BG}} - C_{\mathrm{BG}}. \quad (8)$$

The contamination term was small and only increases to 1% at the lowest x bin. The background dilution also increases at low x and becomes significant ($>$ 10% of the measured asymmetry) only for $x < 0.35$.

After correcting for the pair symmetric background the radiative corrections were applied following the standard formalism laid out by Mo and Tsai [9] and the polarization dependent treatment of Akushevich, et.al. [10]. The elastic radiative tail was calculated from models of the proton form factor [11]. The pair-symmetric background-corrected asymmetry was corrected with elastic dilution and contamination terms

$$A_{el}(\alpha) = A_b(\alpha)/f_{el} - C_{el} \tag{9}$$

where f_{el} is the ratio of inelastic scattering to the sum of elastic and inelastic scattering, and C_{el} is the polarized elastic scattering cross section difference over the total inelastic cross section. The elastic dilution term remained less than 10% of the measured asymmetry in the range $x = 0.3$ to 0.8 for both target configurations. In the same range of x the longitudinal configuration's elastic contamination remained less than 10% in absolute value, whereas, the transverse configuration's elastic contamination remained less than a few percent in absolute units.

The last correction required calculating the polarization dependent inelastic radiative tail of the born-level polarization-dependent cross sections, which form the measured asymmetry. However, numerical studies [9, 12] with various models indicate the size of this radiative tail is small for most kinematics, reaching a few percent only at the lowest and highest E' bins. More importantly, the contribution of this radiative tail to the inelastic asymmetry remains within the systematic uncertainties associated with the model and numerical precision of our calculations. Therefore, this correction was treated as a systematic uncertainty. This situation can only improve with future precision measurements of the polarization-dependent cross sections by scanning beam energies at a fixed angle [9].

The virtual Compton scattering asymmetries can be written in terms of the measured asymmetries

$$\begin{aligned} A_1 = \frac{1}{D'}\Big[&\frac{E - E'\cos\theta}{E + E'}A_{180} \\ &+ \frac{E'\sin\theta}{(E+E')\cos\phi}\frac{A_{180}\cos\alpha + A_\alpha}{\sin\alpha}\Big] \end{aligned} \tag{10}$$

and

$$A_2 = \frac{\sqrt{Q^2}}{2ED'}\Big[A_{180} - \frac{E - E'\cos\theta}{E'\sin\theta\cos\phi}\frac{A_{180}\cos\alpha + A_\alpha}{\sin\alpha}\Big] \tag{11}$$

with $\alpha = 80°$ and where A_{180} and A_{80} are the corrected asymmetries, $D' = (1-\epsilon)/(1+\epsilon R)$, $\epsilon = (1 + 2(1 + \nu^2/Q^2)\tan^2(\theta/2))^{-1}$ is the virtual photon polarization ratio, and $R = \sigma_L/\sigma_T$ is the ratio of longitudinal to transverse unpolarized cross sections. The combined results for A_1 and A_2 versus W are shown in FIG. 1. These results significantly improve the world data on A_2^p.

The spin structure functions can be obtained from the measured asymmetries by using equations (10) and (11) along with

$$g_1 = \frac{F_1}{1+\gamma^2}\left(A_1 + \gamma A_2\right) \tag{12}$$

$$g_2 = \frac{F_1}{1+\gamma^2}\left(A_2/\gamma - A_1\right), \tag{13}$$

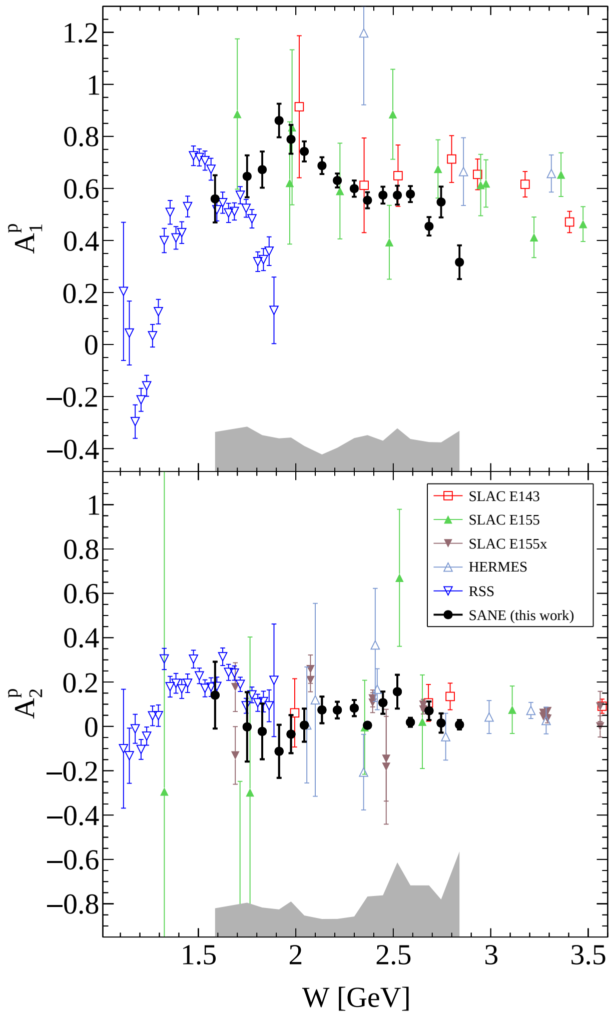

FIG. 1. The SANE results (circle) and existing data from SLAC's E143 (square)[13], E155 (filled up triangle) [14] , E155x (filled down triangle)[15], HERMES (up triangle) [16], and RSS (down triangle) [17] experiments for the virtual Compton scattering asymmetries A_1^p (top) and A_2^p (bottom).

where $\gamma^2 = Q^2/\nu^2$. Additionally, it provides much needed data for both spin structure functions at high x. For $Q^2 <\sim 5$ GeV^2 corrections due to the proton's finite mass become significant and matrix elements of definite twist and spin cannot be extracted from the CN moments. Nachtmann moments, by their construction, select matrix elements of definite twist and spin. At low Q^2, Nachtmann moments should be used instead of the CN moments as emphasized in [18]. Definitions of the Nachtmann moments are found in [18–20] and are related to the reduced matrix elements through

$$M_1^{(n)}(Q^2) = a_n = \frac{\tilde{a}_{n-1}}{2}, \qquad \text{for } n = 1, 3... \tag{14}$$

$$M_2^{(n)}(Q^2) = d_n = \frac{\tilde{d}_{n-1}}{2}, \qquad \text{for } n = 3, 5... \tag{15}$$

TABLE I. Results for the Nachtmann moment M_2^3. Note this reduces to $\tilde{d}_2^p/2$ in absence of target mass corrections.

	$\langle Q^2 \rangle = 2.88$ GeV^2	$\langle Q^2 \rangle = 4.27$ GeV^2
$x_{\mathrm{low}} - x_{\mathrm{high}}$	$0.268 - 0.571$	$0.445 - 0.739$
$M_2^3 \times 10^3$		
total	$-3.17 \pm 0.962 \pm 1.185$	$-0.019 \pm 0.822 \pm 4.17$
measured	$-3.40 \pm 0.962 \pm 0.864$	$-1.71 \pm 0.822 \pm 1.75$
low x	1.22 ± 0.0611	4.16 ± 0.20
high x	-2.33 ± 0.116	-1.83 ± 0.0915
elastic	-0.0281 ± 0.251	-0.133 ± 0.126

where we use the convention of Dong[1]. When the target mass is neglected, i.e. $M^2/Q^2 \to 0$, these equations reduce to $M_1^1 = \int g_1 dx$ and $2M_2^3 = \int x^2(2g_1 + 3g_2)dx$.

It is important to note that the moments include the point at $x = 1$ which corresponds to elastic scattering on the nucleon. The elastic contributions to the moments are computed according to [26] using empirical fits to the electric and magnetic form factors [11]. At large Q^2 the elastic contribution becomes negligible. In some sense the elastic contribution, $\tilde{d}_2^{el}$, is of little interest – it is the deviation from the elastic which provides the insight into the color forces responsible for confinement.

The results for the Nachtmann moment $2M_2^{(3)}(Q^2) = \tilde{d}_2(Q^2)$ are shown in FIG. 2 along with a comparison to the two previous measurements, lattice results, and model calculations. The first measurement was extracted from the combined results of the SLAC E143, E155, and E155x experiments[15]. The SLAC and lattice results are in agreement with our result at $Q^2 = 4.4$ GeV^2. The measurement from the Resonance Spin Structure (RSS) experiment [17], extracted at $Q^2 = 1.28$ GeV^2 a value $\tilde{d}_2^p = 0.0104 \pm 0.0016$, of which $\sim 1/3$ comes from the inelastic contribution.

At $Q^2 = 2.9$ the result is lower than the elastic and next-to-leading power corrections predict. Interestingly, this result complements a recent neutron $\tilde{d}_2^n$ measurement [27] which also observed a significantly more negative value at $Q^2 \simeq 3$ GeV^2. Taken together, these results may indicate the forces observed are iso-spin independent. Interpreted as an average color Lorentz force, this observation agrees with simple model that the proton and neutron, being iso-spin partners, have the same color-space wave-function, and therefore, the struck quark will feel the same average color force.

[1] Some authors define the matrix elements excluding a factor of 1/2[19, 21–23], and/or use even n for the moments [24, 25]. In this work we use the convention of [18, 20] which absorbs the 1/2 factor into the matrix element and use odd n for the moments, whereas, the matrix elements excluding the 1/2 and even n are $\tilde{a}_{n-1}$ and $\tilde{d}_{n-1}$.

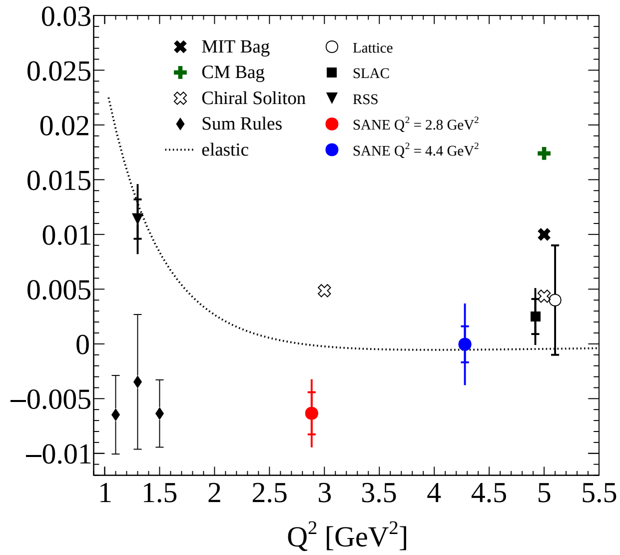

FIG. 2. The SANE results (filled circles) for $2M_2^3 \simeq \tilde{d}_2^p$. The lattice result (open circle) [6] and previous measurements from SLAC [15] and RSS [17, 28] are shown with the dotted line corresponding to the elastic contribution. Model calculations from sum rules [29, 30], the CM bag model [30, 31], and the chiral soliton model [32] are also shown.

In summary, the proton's spin structure functions g_1 and g_2 have been measured at kinematics allowing for an extraction of two $\tilde{d}_2$ values each at near constant Q^2. The present results may indicate that the color Lorentz force may have a non-trivial scale dependence. This scale dependence may shed light on quark-gluon correlations of QCD responsible for the partonic structure of the nucleon. In the future, precision measurements with a transversely polarized proton target will greatly improve our understanding of these color forces.

[1] R. L. Jaffe, in *The spin structure of the nucleon. Proceedings, International School of Nucleon Structure, 1st Course, Erice, Italy, August 3-10, 1995* (1996) pp. 42–129, arXiv:hep-ph/9602236 [hep-ph].
[2] M. Burkardt, *Proceedings, Workshop on Spin structure at long distance: Newport News, USA, March 12-13, 2009*, AIP Conf. Proc. **1155**, 26 (2009), arXiv:0905.4079 [hep-ph].
[3] M. Burkardt, in *Proceedings, 4th Workshop on Exclusive Reactions at High Momentum Transfer: Newport News, USA, May 18-21, 2010* (2011) pp. 101–110, arXiv:1009.5442 [hep-ph].
[4] A. Accardi, A. Bacchetta, W. Melnitchouk, and M. Schlegel, JHEP **11**, 093 (2009), arXiv:0907.2942 [hep-ph].
[5] R. L. Jaffe, Comments Nucl. Part. Phys. **19**, 239 (1990).
[6] M. Gockeler, R. Horsley, W. Kurzinger, H. Oelrich, D. Pleiter, P. E. L. Rakow, A. Schafer, and G. Schierholz,

Phys. Rev. **D63**, 074506 (2001), arXiv:hep-lat/0011091 [hep-lat].

[7] J. D. Maxwell *et al.*, Nucl. Instrum. Meth. **A885**, 145 (2018), arXiv:1711.09089 [physics.ins-det].

[8] W. R. Armstrong, S. Choi, E. Kaczanowicz, A. Lukhanin, Z.-E. Meziani, and B. Sawatzky, Nucl. Instrum. Meth. **A804**, 118 (2015), arXiv:1503.03138 [physics.ins-det].

[9] L. W. Mo and Y.-S. Tsai, Rev. Mod. Phys. **41**, 205 (1969).

[10] I. V. Akushevich and N. M. Shumeiko, J. Phys. **G20**, 513 (1994).

[11] J. Arrington, W. Melnitchouk, and J. A. Tjon, Phys. Rev. **C76**, 035205 (2007), arXiv:0707.1861 [nucl-ex].

[12] I. Akushevich, A. Ilyichev, N. Shumeiko, A. Soroko, and A. Tolkachev, Comput. Phys. Commun. **104**, 201 (1997), arXiv:hep-ph/9706516 [hep-ph].

[13] K. Abe *et al.* (E143), Phys. Rev. Lett. **78**, 815 (1997), arXiv:hep-ex/9701004 [hep-ex].

[14] P. L. Anthony *et al.* (E155), Phys. Lett. **B458**, 529 (1999), arXiv:hep-ex/9901006 [hep-ex].

[15] P. L. Anthony *et al.* (E155), Phys. Lett. **B553**, 18 (2003), arXiv:hep-ex/0204028 [hep-ex].

[16] A. Airapetian *et al.* (HERMES), Eur. Phys. J. **C72**, 1921 (2012), arXiv:1112.5584 [hep-ex].

[17] K. Slifer *et al.* (Resonance Spin Structure), Phys. Rev. Lett. **105**, 101601 (2010), arXiv:0812.0031 [nucl-ex].

[18] Y. B. Dong, Phys. Rev. **C78**, 028201 (2008), arXiv:0811.1002 [hep-ph].

[19] S. Matsuda and T. Uematsu, Nucl. Phys. **B168**, 181 (1980).

[20] A. Piccione and G. Ridolfi, Nucl. Phys. **B513**, 301 (1998), arXiv:hep-ph/9707478 [hep-ph].

[21] J. Kodaira, S. Matsuda, T. Muta, K. Sasaki, and T. Uematsu, Phys. Rev. **D20**, 627 (1979).

[22] J. Kodaira, Nucl. Phys. **B165**, 129 (1980).

[23] J. Kodaira, S. Matsuda, K. Sasaki, and T. Uematsu, Nucl. Phys. **B159**, 99 (1979).

[24] R. L. Jaffe and X.-D. Ji, Phys. Rev. **D43**, 724 (1991).

[25] J. Blumlein and A. Tkabladze, Nucl. Phys. **B553**, 427 (1999), arXiv:hep-ph/9812478 [hep-ph].

[26] W. Melnitchouk, R. Ent, and C. Keppel, Phys. Rept. **406**, 127 (2005), arXiv:hep-ph/0501217 [hep-ph].

[27] M. Posik *et al.* (Jefferson Lab Hall A), Phys. Rev. Lett. **113**, 022002 (2014), arXiv:1404.4003 [nucl-ex].

[28] F. R. Wesselmann *et al.* (RSS), Phys. Rev. Lett. **98**, 132003 (2007), arXiv:nucl-ex/0608003 [nucl-ex].

[29] I. I. Balitsky, V. M. Braun, and A. V. Kolesnichenko, Phys. Lett. **B242**, 245 (1990), [Erratum: Phys. Lett.B318,648(1993)], arXiv:hep-ph/9310316 [hep-ph].

[30] E. Stein, P. Gornicki, L. Mankiewicz, A. Schafer, and W. Greiner, Phys. Lett. **B343**, 369 (1995), arXiv:hep-ph/9409212 [hep-ph].

[31] X. Song, Phys. Rev. **D54**, 1955 (1996), arXiv:hep-ph/9604264 [hep-ph].

[32] H. Weigel, L. P. Gamberg, and H. Reinhardt, Phys. Rev. **D55**, 6910 (1997), arXiv:hep-ph/9609226 [hep-ph].